Macromolecules

Article

pubs.acs.org/Macromolecules

Theoretical Study of Phase Behavior of Frustrated ABC Linear Triblock Copolymers

Meijiao Liu, Weihua Li,* and Feng Qiu

State Key Laboratory of Molecular Engineering of Polymers, Department of Macromolecular Science, Fudan University, Shanghai 200433, China

An-Chang Shi

Department of Physics and Astronomy, McMaster University, Hamilton, Ontario, Canada L8S 4M1

ABSTRACT: The self-assembling behavior of ABC linear triblock copolymer melts is systematically studied using the self-consistent field theory, focusing on the emergence and stability of the knitting-pattern (KP) phase. The KP is one of the most intriguing unconventional phases formed from "frustrated" linear triblock copolymers, where the interaction between the two end blocks is much weaker than those between neighboring blocks. Specifically phase diagrams for linear ABC triblock copolymer melts are constructed by comparing the free energy of about 10 candidate structures, including the knitting patterns, three-color lamellae (L_3), core−shell cylinders (CSC), perforated lamellae (PL), cylinders-within-lamellae (LC), triple/quadruple cylinders-on-cylinders (C_3/C_4), double/triple helices-on-cylinders (H_2C/H_3C), and perforated circular lamella-on-cylinders (PC). The results of the phase behavior are presented for three cases with increasing complexity of the block copolymers. First of all, we investigate the stable region of the KP phase in triblock copolymers with a uniform segment size. Second, we study the impact of the conformational parameters as well as the interaction asymmetry between neighboring blocks on the stability of the KP phase. Finally, we examine the stability region of the KP phase surrounded by LC, PL, L_3, CSC, PC, and C_4 phases for a model system with a specific set of parameters corresponding to those of the polystyrene−poly(ethylene-*co*-butylene)−poly(methyl methacrylate) (PS−PEB−PMMMA) samples.

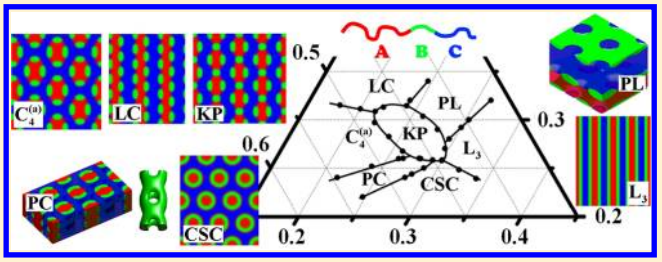

I. INTRODUCTION

Block copolymers have attracted increasing attention due to their ability to self-assemble into a variety of ordered nanoscale structures. From a technological point of view these nanostructures can serve as templates and scaffolds for generating porous materials,[1] sectoring floating gates in flash memory,[2] ultrahigh density magnetic storage media,[3] photovoltaic devices,[4] etc. From a fundamental point of view the rich phase behavior of block copolymers provides a paradigm for the study of phases and phase transitions of soft condensed matter. The rich phase behavior is demonstrated by diblock copolymers, which are the simplest block copolymers composed of two chemically different blocks linked at their ends. It has been well established that diblock copolymers can self-assemble into a number of stable phases including lamellae, gyroids, cylinders, spheres, and the *Fddd* network.[5,6] An enormous number of ordered phases with increased complexities can be formed by more complex block copolymers with multiblocks and/or different topologies. For example, adding one chemically distinct C block to an AB diblock copolymer leads to ABC triblock copolymers. Compared with AB diblock copolymers, ABC triblock copolymers have more independent parameters controlling their phase behavior. In general, the phase behavior of AB diblock copolymers is controlled mainly by three parameters: the volume fraction of the A-blocks f, the interaction strength characterized by the product χN where N is the degree of polymerization of the chain and χ is the Flory−Huggins interaction parameter between the A and B monomers, and a parameter quantifying the conformational asymmetry arising from the different segment sizes. For ABC triblock copolymers, the number of parameters increases to seven, including three interaction parameters $\chi_{AB}N$, $\chi_{BC}N$, and $\chi_{AC}N$; two independent volume fractions f_A and f_B; and two independent conformational parameters. In addition, different chain architectures, i.e. linear, star,[7] or ring,[8] can also enrich their phase behavior dramatically. This seven-dimensional parameter space makes ABC triblock copolymers be a great model system for engineering of a large number of intriguing nanostructures. At the same time, the complexity of the self-assembling behaviors of ABC triblock copolymers makes the exploration of their phase diagrams a formidable task. For example, our understanding of the phase behavior of linear

Received: September 29, 2012
Revised: November 7, 2012
Published: November 15, 2012

dx.doi.org/10.1021/ma302060m | *Macromolecules* 2012, 45, 9522−9530

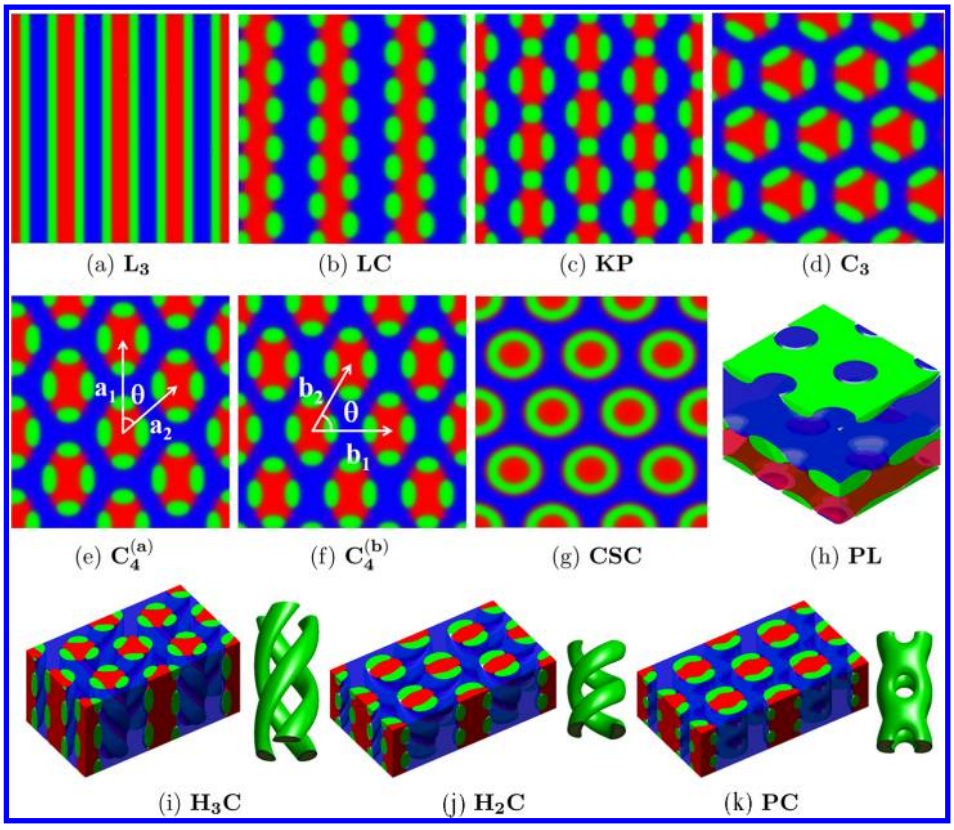

Figure 1. Density isosurface plots of morphologies formed by ABC linear triblock copolymers: (a) three-color lamellae (L_3), (b) cylinders-within-lamellae (LC), (c) knitting pattern (KP), (d) triple cylinders-on-cylinders (C_3), (e) and (f) quadruple cylinders-on-cylinders ($C_4^{(a)}$ and $C_4^{(b)}$, their difference is explained in the text), (g) core−shell cylinders (CSC), (h) perforated lamellae (PL), (i) triple helices-on-cylinders (H_3C), (j) double helices-on-cylinders (H_2C), and (k) perforated circular layer-on cylinders (PC). In $C_4^{(a)}$ and $C_4^{(b)}$, their basis vectors are indicated. The red, green, and blue colors denote the regions where the majority components are A, B, and C, respectively.

ABC triblock copolymers, the simplest ABC triblock copolymers, is still incomplete.

Generically, the phase behavior of linear ABC triblock copolymer melts can be classified into "nonfrustrated" and "frustrated" cases according to the relative strength of the three Flory−Huggins interaction parameters.[9] In the nonfrustrated case, the interaction between the two end-blocks, $\chi_{AC}N$, is comparable to or larger than those between neighboring blocks, $\chi_{AB}N$ and $\chi_{BC}N$. Therefore, the A and C blocks prefer to be separated, forming distinct A/B and B/C interfaces. The domain arrangement in this type of structures is consistent with the topology of block sequence in the linear ABC copolymer. In the frustrated case, $\chi_{AC}N$ is much weaker than $\chi_{AB}N$ and $\chi_{BC}N$. Thus, the triblock copolymers prefer to form structures with A/C interfaces, which have lower interfacial energy that the A/B and B/C interfaces. However, the formation of A/C interfaces is not commensurate with the chain topology; thus, the system is frustrated. The delicate balance between the benefit of interfacial energy and the energy penalty due to the topological constraints leads to the formation of complex ordered phases, in which the topological frustration is partially alleviated.

Experimentally, a number of frustrated triblock copolymer systems have been studied by a number of groups, including poly(styrene-*block*-butylene-*block*-methyl methacrylate) (SBM)[10−16] and its partially hydrogenated analogue poly(styrene-*block*-ethylene-*co*-butylene-*block*-methyl methacrylate) (SEBM)[10,12−14,17−19] as well as poly(styrene-*block*-2-vinylpyridine-*block*-*tert*-butyl methacrylate) (SVT)[20−23] and poly(styrene-*block*-butadiene-*block*-caprolactone) (SBC).[24] A large number of complex structure-within-structure phases, including cylinders-within-lamellae, spheres-within-lamellae, cylinders-on-cylinders, helices-on-cylinders, rings-on-cylinders, spheres-on-cylinders, spheres-on-spheres, and knitting patterns have been observed in these systems. These complex phases are typical hierarchical structures because at least two lengths are required to characterize them.

Besides the experimental studies, the self-assembly of frustrated triblock copolymers has been investigated by computer simulations and theoretical calculations. Computer simulations often play important roles in the study of block copolymer self-assemblies, especially in identifying previously unknown structures. Recently, Nagpal et al. have systematically studied the self-assembly of linear ABC triblock copolymers, including both nonfrustrated and frustrated cases, using Monte Carlo (MC) simulations.[25] In their simulations, most of frustrated morphologies have translational symmetry along one direction, representing two-dimensional (2D) phases. On the theory side, an important contribution is the study of phase diagrams of SEBM by Zheng and Wang[26] using the strong segregation theory (SST), where the interaction parameters were chosen as χ_{AB}:χ_{BC}:χ_{AC} = 1:3.61:0.09. In their SST calculations, three frustrated phases, the cylinders-within-lamellae, spheres-within-lamellae, and rings-on-cylinders, were examined. Another powerful theoretical framework for the study of polymeric systems is the self-consistent field theory (SCFT). An early SCFT study has been carried out to examine the phase behavior of frustrated triblock copolymers by Tang et

dx.doi.org/10.1021/ma302060m | *Macromolecules* 2012, 45, 9522−9530

al.[27] Specifically they constructed phase diagrams using two-dimensional (2D) phases as candidate structures. The restriction to 2D phases for frustrated ABC triblock copolymers was alleviated later by Guo et al.[28] using a generic spectral method to solve the SCFT equations. These authors constructed a comprehensive triangular phase diagram for the ABC linear triblock copolymers with $\chi_{AB}N = \chi_{BC}N = 35$ and $\chi_{AC}N = 15$. In general, a large number of basis functions are required to describe a well-ordered morphology and to determine its free energy by this spectral method, particularly for the hierarchical phases. Because of the limited number of basis functions used in the construction of the phase diagram, the accuracy of the phase boundaries obtained by Guo et al. is limited. Further discussion about the effect of the number of basis functions on the relative stability between phases will be given in the Results and Discussion section. A more accurate phase diagram is required to understand the complicated self-assembling behavior of frustrated triblock copolymers. Very recently, Li et al.[29] have studied the phase behavior of supercylinder-forming ABC triblock copolymers using full 3D pseudospectral method of SCFT. The supercylinder morphology is composed of hexagonally arranged cylinders formed by the minority end-blocks; each of these cylinders is decorated by substructures, including triple/quadruple cylinders, single/double/triple helices, rings, spheres, and perforated circular layer, formed from the middle blocks. The phase diagrams, constructed by comparing free energy of candidate phases, predict that double and triple helices-on-cylinder phases are stable and rings-on-cylinders, single helix-on-cylinders, and triple/quadruple cylinders-on-cylinders phases are metastable. In addition, it is also revealed that the relative rotation and chirality between two neighboring helical supercylinders can affect their relative stability. The prediction that the opposite chirality is preferred by neighboring helical supercylinders is well consistent with recent experimental observations.[16]

One of the many self-assembled morphologies of frustrated triblock copolymers is the knitting pattern (KP), consisting of peristaltic lamellae formed by one end blocks, in which opposite maxima and minima are spanned by ellipse-shaped cylindrical domains formed by the middle blocks (Figure 1c). In early experiments, the KP morphology was first observed in a $S_{35}EB_{27}M_{38}$ sample by Breiner et al.,[12] and the two-dimensional space group was identified as *c2mm* by the transmission electron microscopy(TEM) images.[17] In their studies, the KP phase is formed in hydrogenated SBM samples but not in non-hydrogenated ones, and it can be obtained from the chloroform ($CHCl_3$) casting solvent but not from that of toluene. On the basis of these observations, Breiner et al. speculated that the KP structure is an intermediate morphology between the three-color lamellae (L_3) and the cylinders-within-lamellae (LC).[12,17] Subsequently, Ott and co-workers carried out a systematic exploration of the KP morphology throughout the composition region of SEBM samples, where the KP morphology was obtained, but was speculated as a metastable phase, within the region of $f_B \approx 0.30-0.32$ and $f_A \approx 0.30-0.37$.[19] All of these experimental results reveal that the KP phase is neighbored by the L_3 and LC phases. In contrast to the experimental studies, the KP morphology has been observed in very few theoretical studies,[28,30,31] particularly for the frustrated ABC linear triblock copolymers.[28] To our best knowledge, the KP phase of ABC linear triblock copolymer was only obtained in the SCFT calculations with interaction parameters of $\chi_{AB}N = 27$, $\chi_{BC}N = 59$, and $\chi_{AC}N = 11.5$; compositions of $(f_A, f_B, f_C) = (0.36, 0.31, 0.33)$; and distinct segment lengths of $b_A = 0.61$ nm, $b_B = 0.68$ nm, and $b_C = 0.65$ nm.[28] This theoretical result suggests that the conformational asymmetry, due to the different segment sizes, of the copolymers may be an important factor to the formation of the KP phase. It should also be noticed that the shape of the KP morphology in Figure 3 of ref 28 is quite different from those in experiments. In particular, the B-domains on the locations of minima or maxima of the oppositely wavy C-lamellae are noticeably elongated. In addition, the stability of the KP morphology has not been identified in previous SCFT calculations. In this paper we fill this gap by carrying out a systematic study of the stability of the KP phase in linear ABC triblock copolymers using the pseudospectral method of SCFT, which is the method of choice for the study of block copolymer complex phases.[29] Our study of the KP phase is motivated by the large number of available experimental observation of this structure, and thus our results can be compared with experiments directly. Furthermore, the KP phase is an intermediate structure between the simple ABC lamellae and the cylinder-within-lamellae. Therefore, the KP phase is an excellent example to study the effect of frustration due to the monomer interactions and topological constraint. The theoretical results from the current study can be used to gain a good understanding of the self-assembly mechanism and the relative stability of the different complex phases. In particular, it is essential to explore as many as possible neighboring phases of the KP phase. For example, the decreased volume fraction of the A-blocks would induce the A-domains in the KP morphology to transform to cylinders, leading to the transition of the KP phase to the supercylinder phases. Therefore, the frustrated supercylinder phases considered in our previous work are useful candidates as competing phases.[29]

In experiments, it has been revealed that the formation of the KP phase is sensitive to the characteristics of each block of the triblock copolymers, including the compositions, the immiscibility between the three components, and the conformational parameters. For example, the property of the middle B-block in the SBM triblock copolymers is altered by hydrogenation or different solvent environments. In this work, we focus on the determination of the KP phase stability in frustrated ABC linear triblock copolymers using the pseudospectral method of SCFT. Specifically three cases with increasing complexities are used to illustrate the phase behavior. First of all, we investigate ABC triblock copolymers assuming the A, B, and C segments have the same size. Second, we study the impact of conformational parameters as well as the interaction asymmetry between $\chi_{AB}N$ and $\chi_{BC}N$ on the stability of the KP phase. Finally, we choose a specific set of parameters corresponding to the SEBM triblock copolymers and identify the stability region of the KP phase surrounded by its neighboring phases in the triangular phase diagram.

II. THEORY AND METHOD

We consider an incompressible melt of ABC linear triblock copolymers in a volume of V. Each copolymer chain is specified by the degrees of polymerization of the blocks, Z_A, Z_B, and Z_C, and each block is characterized by the segment length b_K and density ρ_K (K = A, B, C). The repulsive interactions between different monomers are characterized by three Flory–Huggins parameters χ_{AB}, χ_{BC}, and χ_{AC}, respectively. For convenience, a reference density ρ_0 is introduced to define the effective degree of polymerization of the triblock copolymer chain, $N = N_A + N_B$

+ N_C. Specifically, N is defined such that the product of $N\rho_0^{-1}$ is equal to the volume occupied by a single copolymer chain, $N\rho_0^{-1} = Z_A\rho_A^{-1} + Z_B\rho_B^{-1} + Z_C\rho_C^{-1}$. The volume fraction of block K is then given by $f_K = N_K/N$ ($f_A + f_B + f_C = 1$). Besides the interaction parameters, the different blocks are further characterized by their conformational asymmetry. It has been proposed that the conformational asymmetry can be parametrized by the ratio[32]

$$\varepsilon_K = \left(\frac{\beta_K}{\beta_A}\right)^2 \tag{1}$$

where β_K are quantities characterizing the flexibilities of different blocks which can be defined by the combination of pure component parameters

$$\beta_K^2 \equiv \frac{R_{g,K}^2}{Z_K\rho_K^{-1}} = \frac{b_K^2\rho_K}{6} \tag{2}$$

In this expression, $R_{g,K}^2 = Z_K b_K^2/6$ is the square of the unperturbed radius of gyration of block K. In the definition of eq 1, the A-monomer is chosen as the reference; thus $\varepsilon_A = 1$. Substituting the expression of β_K into eq 1, the conformational asymmetry parameter becomes

$$\varepsilon_K = \frac{b_K^2\rho_K}{b_A^2\rho_A} \tag{3}$$

Therefore, the conformational asymmetry is quantified by the combination of statistical segment size and segment density. The effect of this conformational asymmetry on the phase behavior of ABC triblock copolymers is one of our focuses in this work.

Within the mean-field approximation to statistical mechanics of the Edwards model of polymers,[33,34] the free energy functional F of n Gaussian triblock copolymer chains at a given temperature T is given by

$$\begin{aligned}\frac{F}{nk_BT} = -\ln Q + \frac{1}{V}\int d\mathbf{r}\{&\chi_{AB}N\phi_A(\mathbf{r})\phi_B(\mathbf{r}) \\ &+ \chi_{AC}N\phi_A(\mathbf{r})\phi_C(\mathbf{r}) + \chi_{BC}N\phi_B(\mathbf{r})\phi_C(\mathbf{r}) \\ &- w_A(\mathbf{r})\phi_A(\mathbf{r}) - w_B(\mathbf{r})\phi_B(\mathbf{r}) - w_C(\mathbf{r})\phi_C(\mathbf{r}) \\ &- \eta(\mathbf{r})[1 - \phi_A(\mathbf{r}) - \phi_B(\mathbf{r}) - \phi_C(\mathbf{r})]\}\end{aligned} \tag{4}$$

where ϕ_K (K = A, B, and C) are the monomer densities. The quantity Q is the partition function of a single polymer chain interacting with the mean fields of w_K, which are produced by the surrounding chains. The field function $\eta(\mathbf{r})$ is a Lagrange multiplier used to enforce the incompressibility conditions, $\phi_A(\mathbf{r}) + \phi_B(\mathbf{r}) + \phi_C(\mathbf{r}) = 1$. Minimization of the free energy with respect to the monomer densities and the mean-fields leads to the following SCFT equations:

$$w_A(\mathbf{r}) = \chi_{AB}N\phi_B(\mathbf{r}) + \chi_{AC}N\phi_C(\mathbf{r}) + \eta(\mathbf{r}) \tag{5}$$

$$w_B(\mathbf{r}) = \chi_{AB}N\phi_A(\mathbf{r}) + \chi_{BC}N\phi_C(\mathbf{r}) + \eta(\mathbf{r}) \tag{6}$$

$$w_C(\mathbf{r}) = \chi_{AC}N\phi_A(\mathbf{r}) + \chi_{BC}N\phi_B(\mathbf{r}) + \eta(\mathbf{r}) \tag{7}$$

$$\phi_A(\mathbf{r}) = \frac{1}{Q}\int_0^{f_A} ds\, q(\mathbf{r}, s)q^\dagger(\mathbf{r}, s) \tag{8}$$

$$\phi_B(\mathbf{r}) = \frac{1}{Q}\int_{f_A}^{f_A+f_B} ds\, q(\mathbf{r}, s)q^\dagger(\mathbf{r}, s) \tag{9}$$

$$\phi_C(\mathbf{r}) = \frac{1}{Q}\int_{f_A+f_B}^{1} ds\, q(\mathbf{r}, s)q^\dagger(\mathbf{r}, s) \tag{10}$$

$$Q = \frac{1}{V}\int d\mathbf{r}\, q(\mathbf{r}, s)q^\dagger(\mathbf{r}, s) \tag{11}$$

$$\phi_A(\mathbf{r}) + \phi_B(\mathbf{r}) + \phi_C(\mathbf{r}) = 1 \tag{12}$$

In the above equations, $q(\mathbf{r},s)$ and $q^\dagger(\mathbf{r},s)$ are the end-segment distribution functions.[34] These distribution functions satisfy the modified diffusion equations

$$\frac{\partial q(\mathbf{r}, s)}{\partial s} = \varepsilon(s)\nabla^2 q(\mathbf{r}, s) - w(\mathbf{r}, s)q(\mathbf{r}, s) \tag{13}$$

$$-\frac{\partial q^\dagger(\mathbf{r}, s)}{\partial s} = \varepsilon(s)\nabla^2 q^\dagger(\mathbf{r}, s) - w(\mathbf{r}, s)q^\dagger(\mathbf{r}, s) \tag{14}$$

where $w(\mathbf{r},s) = w_A(\mathbf{r})$, $\varepsilon(s) = \varepsilon_A$ for $s < f_A$; $w(\mathbf{r},s) = w_B(\mathbf{r})$, $\varepsilon(s) = \varepsilon_B$ for $f_A \le s < f_A + f_B$; and $w(\mathbf{r},s) = w_C(\mathbf{r})$, $\varepsilon(s) = \varepsilon_C$ for $f_A + f_B \le s < 1$. The initial conditions are $q(r,0) = q^\dagger(r,1) = 1$. In all of these expressions the spatial lengths are expressed in units of an effective radius of gyration, $R_{g,eff}$, defined by $R_{g,eff}^2 = Nb_A^2\rho_A/6\rho_0$. For numerical solutions, we employ the pseudospectral method to solve the modified diffusion equations for the end-segment distribution functions. In our calculations, the ABC linear triblock copolymer chains are placed in a rectangle box with sizes of $L_x \times L_y$ for 2D systems and a rectangular cuboid box of $L_x \times L_y \times L_z$ for 3D systems. Periodic boundary conditions are imposed automatically on each direction of the box within the pseudospectral method. The grid spacing is chosen to be small enough to ensure that the accuracy of the free energy calculation is with an error smaller than 10^{-8}.

III. RESULTS AND DISCUSSION

In the 2D KP morphology described by Breiner et al.,[17] each A-domain is surrounded by four B-cylinders with highly nonuniform mean curvature, and the C-domains are wavy lamellae. These features indicate that the KP phase may compete with those known 2D phases in terms of thermodynamic stability, including ABCBA three-color lamellae (denoted as L_3), A/C-lamellae with B-cylinders located at their interfaces (denoted as LC), periodic A-cylinders decorated by triple/quadruple B-subcylinders in the C-matrix (denoted as C_3/C_4), and A/B core−shell cylinders in the C-matrix (denoted as CSC).[9,12,17,29] In addition, the KP phase also competes with some possible complex 3D phases, such as perforated lamellae with hexagonal holes in B-layers (denoted as PL), B-perforated cylindrical shell on A-cylinders in the C-matrix (denoted as PC), and double/triple B-helices on A-cylinders in the C-matrix (denoted as H_2C and H_3C). Therefore, in this work, the above 10 phases, whose density plots are shown in Figure 1, are used as candidate structures. These phases are obtained in our SCFT calculations using specific initial conditions bearing the symmetry of these phases. The free energy of these phases is obtained from their SCFT solutions, and a comparison of the free energy is used to identify the stability of the KP phase. In order to determine the relative stability of these phases, which usually have rather small free energy difference near their phase boundaries, we need to calculate their free energies with reliable accuracy. In our calculations, one or two unit cells for each

dx.doi.org/10.1021/ma302060m | Macromolecules 2012, 45, 9522−9530

structure are employed, and the calculation box is discretized to $N_x \times N_y = 128 \times 128$ lattice for 2D structures and $N_x \times N_y \times N_z = 128 \times 128 \times 64$ lattice for 3D structures (the axis direction of the supercylinders or the normal direction of the perforated lamellae is regulated along the z direction), and the chain contour is divided into $N_s = 100$ points. In the previous work by Li et al.,[29] it has been assumed that the supercylinder phases, including C_3, C_4, H_2C, H_3C, and PC, possess hexagonal symmetry as the simple hexagonal cylinder phase. However, our new calculations find that, except the C_4 phases, the arrangement of the supercylinders deviates from the perfect hexagonal because the 6-fold rotational symmetry of each supercylinder shape is broken by the decoration of four sub-B-domains. In addition, it is found that there are two nearly degenerate C_4 phases (the superscripts of (a) and (b) are used to distinguish them), both of which have parallelogrammic unit cells of the packing array but have different characteristic angles formed by the two basis vectors. The two basis vectors are indicated as $\mathbf{a}_1$ and $\mathbf{a}_2$ for $C_4^{(a)}$ and as $\mathbf{b}_1$ and $\mathbf{b}_2$ for $C_4^{(b)}$ in Figure 1. Thus, the angle, θ, is determined by $\theta = \cos^{-1}(a_1/2a_2)$ in $C_4^{(a)}$ (or $\theta = \cos^{-1}(b_1/2b_2)$ in $C_4^{(b)}$). For an ideal hexagonal array, the angle between $\mathbf{a}_1$ and $\mathbf{a}_2$ (or between $\mathbf{b}_1$ and $\mathbf{b}_2$) is equal to 60°; otherwise, it has a different value. We found that the angles in both $C_4^{(a)}$ and $C_4^{(b)}$ phases are smaller than 60°, but the former angle has smaller value. In fact, the two phases can be distinguished by one main feature of the alignment of the anisotropic domains coformed by the A and B blocks, which are roughly elliptic. In $C_4^{(a)}$, the major axis of the ellipse is aligned along the basis vector a_1, while the minor axis of the ellipse is aligned along the basis vector b_1 in $C_4^{(b)}$. Specific examples indicating the distinct angle values in the two phases will be given later.

A. The Case of Equal Conformational Parameters. As emphasized above, the phase behavior of ABC triblock copolymers is controlled by a large number of parameters. As a first step in understanding their phase behavior, we consider a simple case in which all blocks of the ABC triblock copolymers have equal conformational parameter. Furthermore, we choose a particular set of the interaction parameters, $\chi_{AB}N = \chi_{BC}N = 60$ and $\chi_{AC}N = 15$. This choice of the interaction parameters represents a typical case of the frustrated triblock copolymers such that $\chi_{AC}N \ll \chi_{AB}N = \chi_{BC}N$. The transition points between the KP phase and its surrounding phases in the triangular phase diagram are determined and plotted as filled circles in Figure 2 (the curves in parts b and c are guides to the eyes). As a comparison, those transition points when only 2D phases, including L_3, LC, C_3, and $C_4^{(a)}$, were considered in the competition are shown as unfilled circles. When 2D phases are the only competing phases, the KP phase occupies a noticeable stable phase region between $f_B = 0.21$ and 0.26. To some extent this feature is consistent with the speculation from the experimental observations, in that the KP phase is an intermediate phase between the L_3 and LC phases.[12,17,19,35] When the 3D phases are included in the competition, the stable phase region of the KP phase vanishes in the triangular phase diagram. Instead, two 3D phases, the PL and PC, become stable phases in this region. It is obvious that the 3D PL phase is intermediate between the L_3 and LC phases when these phases are viewed from the aspect of the corresponding AB or BC diblocks as the volume fraction of the B-block decreases. The phase sequence from L_3, to PL, and then to LC, is characterized by the variation of the A/C interface. Two competing factors driving the phase transitions are the energy benefit from the substitute of the favorable A/C interfaces with the high-energy A/B or B/C interfaces, and the penalty of entropic energy from the topological constrain of chain architecture in the frustrated phases with divided B-domains. Small f_B is favorable to form divided B-domains with less entropic loss and thereby is favorable to form frustrated phases. It should be noticed that the PL phase occupies a considerable region between the L_3 and LC, while there is no stable PL phase in simple diblock copolymers, which is replaced by the gyroid phase.[36] Therefore, the ABC linear triblock copolymers provide a scaffold to fabricate perforated structures. The formation of gyroid phase in the present ABC triblock copolymers is hindered by the dominant A/C blocks, which prefer to form the lamellar domains with low mean curvature. According to the phase diagrams of nonfrustrated triblock copolymers,[6,37,38] where the core−shell and alternative gyroid phases have significant stable regions, the gyroid phases with continuous or interrupted B-domains should also be an important candidates of stable phases. Our calculations suggest that the gyroid phases are not a neighboring phase of the KP phase, and we will discuss their stability in future. Why the PC phase, not the triple-helical phase H_3C, is substituted for the C_3 phase can be understood by the phase diagrams of Figures 2 and 3 in ref 29, where H_3C is located in the phase region of smaller f_A and f_B.

Experimentally, the KP morphology can be obtained from the hydrogenated SBM sample, i.e., SEMB, but not from the non-hydrogened SBM. In fact, hydrogenation is an effective way to modify the repulsive interactions between the middle block and the two end blocks,[12] namely, $\chi_{AB}N$ and $\chi_{BC}N$. To examine their effects on the stability of the KP phase, a phase diagram with respect to f_A and $\chi_{AB}N$ for fixed $\chi_{BC}N = 60$, $\chi_{AC}N = 15$, and $f_B = 0.22$ is constructed and presented in Figure 3. It

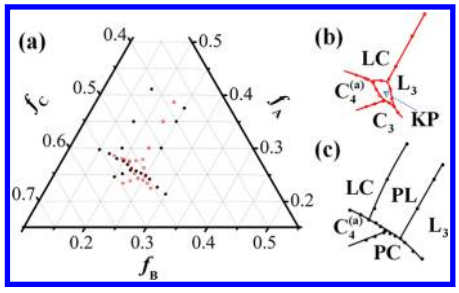

Figure 2. Portion of the triangular phase diagram of the ABC triblock copolymer with equal conformational parameters. The interaction parameters are $\chi_{AB}N = \chi_{BC}N = 60$ and $\chi_{AC}N = 15$. The unfilled circles are determined when only 2D phases are considered, while the filled circles are determined after the 3D phases are included. In (b) and (c), each phase region is indicated, and the curves are guides to the eyes.

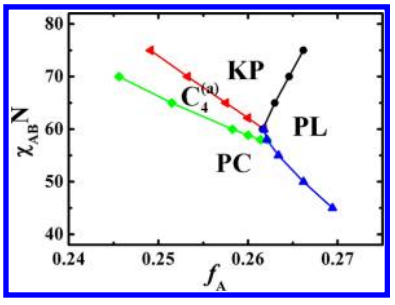

Figure 3. Phase diagram in the f_A−$\chi_{AB}N$ plane for the case of equal conformational parameters with $\chi_{BC}N = 60$, $\chi_{AC}N = 15$, and $f_B = 0.22$.

dx.doi.org/10.1021/ma302060m | Macromolecules 2012, 45, 9522−9530

is interesting to notice that the KP phase becomes stable when $\chi_{AB}N > \chi_{BC}N$, and its stable region is broadened as $\chi_{AB}N$ increases. This prediction seems to be contradictory to the speculation that a weaker A/B interfacial tension than that of B/C favors the formation of the KP phase, which is sketched via the evolution of the KP phase as the volume fraction of the B-blocks increases in the Figure 6 of ref 12. In fact, there is no contradiction between their speculation and our theoretical prediction. The reason is that the main competing phase of KP in the sample of ref 12 with a high volume fraction of A-blocks is LC, while here the competing phases are the $C_4^{(a)}$ and PL phases. The competition between KP and LC will be discussed later. We first take the $C_4^{(a)}$ phase as the main competitor to explain the relative stability of KP. The characteristics of $C_4^{(a)}$ are very similar as those of KP except that each connecting B-domain between two neighboring A-domains is split into a pair, which results in changes of interfacial energy as well as entropic contribution. To analyze quantitatively the relative stability between $C_4^{(a)}$ and KP, we divide the free energy into four parts: three interfacial energies of (U_{AB}, U_{BC}, and U_{AC}), and entropic energy ($-TS$), whose standard definition can be found in ref 39. The differences of the four contributions between $C_4^{(a)}$ and KP are shown in Figure 4b together with the total free energy

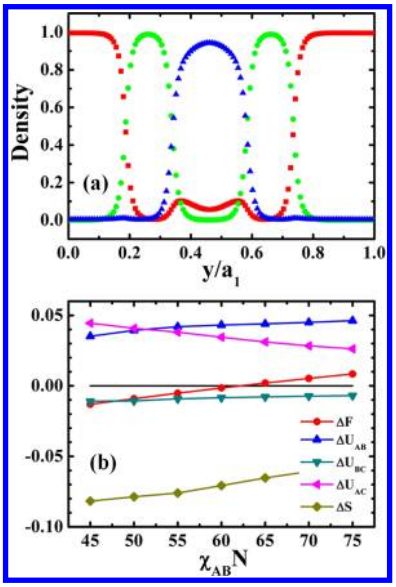

Figure 4. (a) Typical density profiles along the major basis vector a_1 of the $C_4^{(a)}$ phase in Figure 1e. The red, green, and blue symbols represent the density of A, B, and C monomers, respectively. (b) Differences of the free energy as well as all of its contributions between the $C_4^{(a)}$ and KP phases, as a function of $\chi_{AB}N$, for $(f_A, f_B, f_C) = (0.26, 0.22, 0.52)$, $\chi_{BC}N = 60$, and $\chi_{AC}N = 15$. Negative data indicates that $C_4^{(a)}$ has lower value in magnitude.

difference. In the $C_4^{(a)}$ phase, small amount of A-blocks is located at the B/C interfaces around the split B-domains (see the density distribution of Figure 4a along the path indicated by the basis vector of a_1 in Figure 1e) and thus makes the A/B and A/C interfacial energy higher than that of KP (Figure 4b). At the same time, the small amount of A-blocks intermediate between B- and C-domains slightly favors the B/C interfacial energy because of weak A/C interaction. Overall, $C_4^{(a)}$ is less favorable than KP from the total interfacial energy. However, the splitting of the B-domains reduces the topological constraint and thereby adds more available chain configurations into $C_4^{(a)}$. In other words, $C_4^{(a)}$ has lower entropic energy than KP (see Figure 4b). Therefore, the relative stability of KP over $C_4^{(a)}$ is determined by the competition of the two factors: unfavorable entropic energy and favorable interfacial energy. As $\chi_{AB}N$ increases, the superiority of KP in the A/B interfacial energy is amplified, and thus the KP phase becomes more preferred than $C_4^{(a)}$. The change of the relative stability of KP to PL can be understood similarly. From the aspect of composition, increasing A-block favors the formation of the PL phase with low mean curvature of A-domains when C is the largest block in Figure 3. In the other aspect of the interaction parameters, the enhanced $\chi_{AB}N$ enforces more B-components to enter into the C-domains, which induces that A-block tends to form domains with high mean curvature. Therefore, the KP phase becomes more stable than PL at high $\chi_{AB}N$. A brief summary of this discussion is that the KP phase can be tuned to be stable instead of $C_4^{(a)}$ or PL via increasing $\chi_{AB}N$. However, its stability region is rather limited.

B. The Case of Different Conformational Parameters. The chemically distinct blocks found in the experimental samples of triblock copolymers are not only distinguished by their miscibilities but also by their differences in statistical segment properties. The conformational difference of the different segments can also have significant impact on the self-assembling behavior of block copolymers.[40−42] To assess the effect of conformational asymmetry on the phase behavior, the phase diagram with respect to ε_B and f_A, for given $\chi_{AB}N = \chi_{BC}N = 60$, $\chi_{AC}N = 15$, $f_B = 0.22$, and $\varepsilon_C = 1$, is constructed and presented in Figure 5. There are a few notable features in this

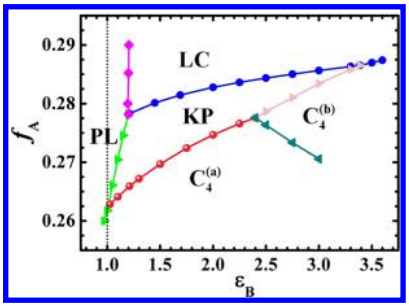

Figure 5. Phase diagram with respect to ε_B and f_A, for $f_B = 0.22$, $\varepsilon_C = 1$, $\chi_{AB}N = \chi_{BC}N = 60$, and $\chi_{AC}N = 15$.

phase diagram. The first one is that when ε_B increases, the PL phase transfers to $C_4^{(a)}$, KP, or LC phase, where the B-domains transform from perforated layers to noncircular cylinders. This is attributed to that increasing the conformational asymmetry ε_B for a fixed f_B can reduce the entropic loss of the B-blocks inside the spontaneous curved domains.[43] Thus, it benefits the formation of interface with a larger mean curvature. This common feature is seen in previous experimental[32] and theoretical[43] studies, where the phase boundaries shift toward larger volume fraction of the block with larger segment size. The second feature is that increasing f_A leads to a stable phase sequence from $C_4^{(a)}$ (or $C_4^{(b)}$), to KP, and then to LC, in the range of $1.0 < \varepsilon_B < 3.4$. Along this phase sequence, the A-blocks first form nearly cylindrical domains in $C_4^{(a)}$ (or $C_4^{(b)}$), then form lamellae by collaborating with the B-blocks in KP, and finally form a complete layer meanwhile repelling B-blocks onto the A/C interfaces in LC. The third feature is that a first-order transition between the two nearly degenerate phases of $C_4^{(a)}$ and $C_4^{(b)}$ is found by varying ε_B. Here we show the different values

dx.doi.org/10.1021/ma302060m | Macromolecules 2012, 45, 9522−9530

of the angle θ in $C_4^{(a)}$ and $C_4^{(b)}$ via specific examples. At ε_B = 2.75, the transition between $C_4^{(a)}$ and $C_4^{(b)}$ in Figure 5 occurs at $f_A \approx 0.2734$. At f_A = 0.27 or 0.28, the value of θ for $C_4^{(a)}$ is around 50.5°, while that for $C_4^{(b)}$ is around 58.0°. From the kinetic aspect of phase transformation, $C_4^{(a)}$ tends to transform to LC by fusing the A-domains along the direction of the basis vector of b_2. Overall, the most important feature of this phase diagram is that the KP phase occupies a noticeable stable region between $1.0 < \varepsilon_B < 3.4$, surrounded by the phases of PL, $C_4^{(a)}$, $C_4^{(b)}$, and LC. This feature directly reveals the important effect of the conformational asymmetry on the relative stability of different phases.

C. Comparison with Experiments. The emergence and stability of the KP phase have been systematically studied by experiments on the SEBM samples, which are categorized into four phase regions in the Figure 2 of ref 19. In two of these regions, the KP phases are observed by solvent casting. The major one, where five samples are examined, is located between 0.34 and 0.37 of the PS composition and between 0.30 and 0.33 of the PEB composition, and the other is centered around (f_{PS}, f_{PEB}, f_{PMMA}) = (0.30, 0.30, 0.40). It was proposed that KP is not an equilibrium structure under the solvent-free conditions in the major area and is metastable in the minor area. The compositional region of the stable KP phase analyzed by our calculations, either in the phase diagram of Figure 3 or in that of Figure 5, is still distinct from those identified in experiments. Our previous calculations suggest that the KP phase can be stabilized by tuning the conformational parameter or the relative values of interaction parameters, i.e., increasing ε_B or $\chi_{AB}N$. Therefore, it may be predicted that we could identify the KP morphology as stable phase in the experimental compositional region by using similar interaction parameters and conformational parameters as those in the experimental samples.

First we analyze the stability of the KP phase with respect to $\chi_{AB}N$ and ε_B for fixed $\chi_{BC}N$ = 60, $\chi_{AC}N$ = 15, ε_C = 1, and composition (f_A, f_B, f_C) = (0.30, 0.30, 0.40) (A: PS; B: PEB; C: PMMA), where the composition is close to that of the experimental sample, $S_{30}EB_{27}M_{43}$, in ref 19. The phase diagram is given in Figure 6, where the KP phase is stable in the region

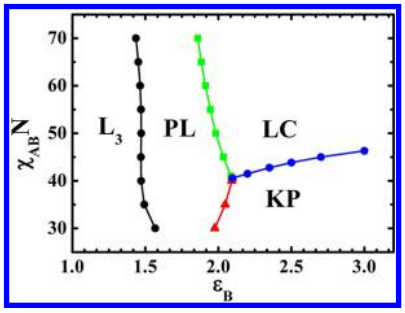

Figure 6. Phase diagram with respect to ε_B and $\chi_{AB}N$ for (f_A, f_B, f_C) = (0.30, 0.30, 0.40), ε_C = 1, $\chi_{BC}N$ = 60, and $\chi_{AC}N$ = 15.

of large ε_B and low $\chi_{AB}N$ via competitions with PL at the direction of decreasing ε_B, and with LC at the direction of increasing $\chi_{AB}N$. The evidence that the KP phase is favorable for low $\chi_{AB}N$ is consistent with the speculation by Breiner et al.[12] but is inconsistent with the result shown in Figure 3. The reason is that the main competing phases of KP in Figure 3 are $C_4^{(a)}$ and PL, but in the current case the competing phases are PL and LC for the present choice of parameters. A transition mechanism between KP and LC as $\chi_{AB}N$ varying has been speculated in Figure 6 of ref 12 that a pair of cylinders on opposite A/C interfaces in LC are squeezed into the A-domain and eventually merge into each other to reduce the A/B interfacial energy and thus to transform to the KP phase as $\chi_{AB}N$ decreases. This explanation is imprecise as compared with the results from our calculations. The comparisons of the different free energy contributions as a function of $\chi_{AB}N$ for ε_B = 2.5 in Figure 7 indicate that the KP phase has higher A/B and

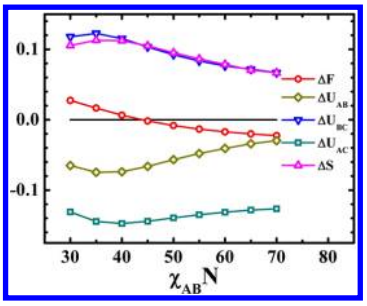

Figure 7. Free energy differences between the phases of LC and KP, as a function of $\chi_{AB}N$, for (f_A, f_B, f_C) = (0.30, 0.30, 0.40), ε_B = 2.5, ε_C = 1, $\chi_{BC}N$ = 60, and $\chi_{AC}N$ = 15.

A/C interfacial energies but more favorable B/C interfacial energy and entropic energy than LC. Therefore, the main merit of the formation of KP is to reduce the B/C interface and the entropic energy at the expense of increasing A/B interface in the situation of low $\chi_{AB}N$. The other transition sequence from L_3 to PL, then to LC or KP, governed by the variation of ε_B, can be readily understood by the change of the mean curvature of B domains induced by ε_B.

The KP phase was first observed in the composition region of (f_A, f_B, f_C) = (0.36, 0.31, 0.33),[12] and it was reproduced with the same parameters in subsequent experiments.[17,19] It is generally believed that larger A-block would induce the transformation of A-domain from near cylinders to layer, namely, the phase transition from KP to LC. To provide a theoretical evidence for this speculation, we examine the relative stability between KP and LC by varying f_A associated with f_C at one phase point adopted from Figure 6 at ε_B = 2.5 and f_B = 0.30. The free energy plots of KP and LC phases as a function of f_A are presented in Figure 8. The result indicates that the KP phase is replaced by LC phase as the stable phase when $f_A \geq 0.33$. With the present choice of parameters, the stability region of the KP phase can be extended toward larger f_A but do not reach the experimental value of f_A = 0.36.

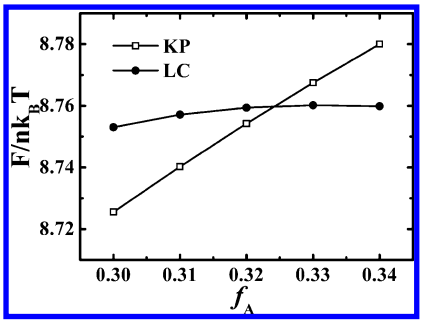

Figure 8. Free energy comparisons between the phases of KP and LC, as a function of f_A, for ε_B = 2.5, ε_C = 1, f_B = 0.30, $\chi_{AB}N$ = 30, $\chi_{BC}N$ = 60, and $\chi_{AC}N$ = 15.

dx.doi.org/10.1021/ma302060m | Macromolecules 2012, 45, 9522−9530

However, we noticed that increasing the difference between $\chi_{AB}N$ and $\chi_{BC}N$ can broaden the stable phase region of KP toward larger value of f_A.

In the present triblock copolymer system, there are at least seven independent controlling parameters, including two composition parameters, three interaction parameters, and two parameters quantifying the conformational asymmetry. To examine the phase behavior of the known sample of SEBM, namely, to construct the triangular phase diagram with respect to the composition, the other five parameters, including $\chi_{AB}N$, $\chi_{AC}N$, $\chi_{BC}N$, ε_B, and ε_C, are required to be specified. Although some qualitative knowledge about the relative strengths between the three interaction parameters is available, their quantitative values are still lacking because of the difficulties in their measurements. For example, it has been proposed that the PS/PMMA interaction is much weaker than that of PS/PEB or PEB/PMMA.[10] However, different values of the Flory–Huggins parameter χ have been presented, such as $\chi_{PS/PMMA}$ = 0.0044 in ref 10 or $\chi_{PS/PMMA}$ = 0.03 in ref 44. Similarly, reliable values for the conformational parameters ε_B and ε_C are not available. The conformational parameter, ε, is determined by the segment length b together with the segment density ρ in eq 3. The common-used data of segment length is b_{PS} = 6.8 Å, b_{PB} = 6.9 Å and b_{PMMA} = 7.4 ± 0.3 Å,[41,45−47] while the segment densities reported in the prior studies are inconsistent, such as the reported values of PS block varying from 5.6 to 6.08, shown in Table 1 of ref 41. Here we choose a specific set of parameters characterizing the main features of the SEBM sample according to relevant reports as $\chi_{AB}N$ = 40, $\chi_{BC}N$ = 80, $\chi_{AC}N$ = 15, ε_B = 2.0, and ε_C = 1.5. The portion of the triangular phase diagram centering around the KP phase is constructed and shown in Figure 9. It reveals that the stable KP phase, surrounded by LC,

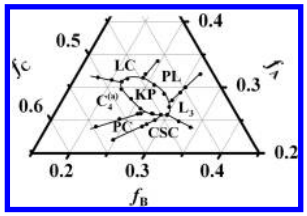

Figure 9. Portion of triangular phase diagram for ε_B = 2.0, ε_C = 1.5, $\chi_{AB}N$ = 40, $\chi_{BC}N$ = 80, and $\chi_{AC}N$ = 15.

PL, L_3, CSC, PC, and $C_4^{(a)}$, is located within the region of f_A = 0.21−0.32 and f_B = 0.21−0.30. There is a small shift toward lower composition of both A- and B-blocks than that estimated in experiments by Ott et al.[19] This discrepancy could be accounted for by a few possible factors. First, our theoretical sample consisting of pure triblock copolymer melts is obviously different from that in experiments. In fact, the formation of the KP morphology in experiments is sensitive to the casting solvent. For example, the KP morphology was observed in the two composition regions by the $CHCl_3$ solvent casting (the major and minor regions discussed previously); however, it was observed only in the minor region with obvious lower A and B compositions by a combining procession of $CHCl_3$ solvent casting and molding compression, which is closer to our phase diagram. When the solvent is replaced by toluene or THF in the solvent casting, the stable phase transfers to L_3.[12,17] Second, the stable phase region of KP is indicated in our phase diagram, whereas KP is claimed as metastable in experiments. Third, the discrepancy of these parameters between theory and experiment is inevitable. Other possible reasons include the polymer polydispersity, small compositiondeviations induced by experimental measurements, and some uncontrollable experimental conditions.

We have mentioned that the number of basis functions has a significant impact on the relative stability between two neighboring phases. Here we take a 2D example to illustrate this impact, i.e., the subtle transitions between $C_4^{(a)}$, KP, and LC, along the phase path of fixed ε_B = 2.0 in Figure 5. To keep the grid spacings in x and y directions close, we set the space lattice as $N_x \times N_x/2$ for the unit cell and choose N_x as 32, 64, 128, and 256. In the pseudospectral method, the number of cosine basis functions is $N_x^2/8$, which are 128, 512, 2048, and 8192 for above values of N_x, respectively. Without considering the error induced by the discretization of the contour length, N_s, the accuracy is comparable to that of the generic spectral method, where the cosine basis functions are applied for centrosymmetric phases. To estimate the error induced by N_s, we examine two values of $N_s = 10^2$ and $N_s = 10^3$. In Figure 10,

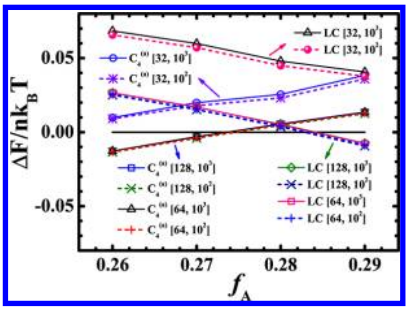

Figure 10. Plots of the free energy of $C_4^{(a)}$ and LC phases relative to the KP phase with f_B = 0.22, ε_B = 2.0, ε_C = 1.0, $\chi_{AB}N = \chi_{BC}N$ = 60, and $\chi_{AC}N$ = 15 for various space lattices $N_x \times N_x/2$ and the contour discretization N_s. The free energy curves of either $C_4^{(a)}$ or LC are nearly overlapped for the parameter groups of $[N_x, N_s]$, [128, 10^3], [128, 10^2], [64, 10^3], and [64, 10^2].

we present the free energy of $C_4^{(a)}$ and LC phases relative to the KP phase with f_B = 0.22, ε_B = 2.0, ε_C = 1.0, $\chi_{AB}N = \chi_{BC}N$ = 60, and $\chi_{AC}N$ = 15 for various groups of parameters $[N_x, N_s]$. Obviously, except for the groups of N_x = 32 with either $N_s = 10^2$ or $N_s = 10^3$, these free energy curves of each phase, $C_4^{(a)}$ or LC, are almost overlapped. In other words, the data of N_x = 64 and N_x = 128 give very similar phase transitions between the three phases, but those of N_x = 32 give incorrect results, where the stability region of KP phase has been expanded many times. This feature implies two points. The first point is that the effect of the contour divisions on the relative stability between two neighboring phases is negligible when $N_s \geq 10^2$ for the current segregation degree of phase separation. The second one is that the size of the space lattice has a significant impact on the accuracy of free energy and thus on the relative stability of phases. In ref 28, the number of cosine basis functions used to search for the KP phase is only 160, which is only slightly larger that 128 of N_x = 32 in our calculations. For 3D phases, the problem because of the limited number of basis functions becomes disastrously serious. This is why it is impossible to observe well-defined 3D morphologies using the generic spectral method, such as the helical supercylindrical phases.

dx.doi.org/10.1021/ma302060m | Macromolecules 2012, 45, 9522−9530

IV. CONCLUSIONS

In summary, we have systematically studied the relative stability of the KP phase in frustrated ABC linear triblock copolymers using SCFT calculations. The free energy of KP is compared with those of 10 competing ordered phases to identify its stable phase region. Our results indicate that the stable phase region of the KP phase is very small or even nonexistent in the case of equal conformational parameters and symmetric interactions of $\chi_{AB}N = \chi_{BC}N = 60$ for $\chi_{AC}N = 15$. When an asymmetry is introduced into $\chi_{AB}N$ and $\chi_{BC}N$, i.e., $\chi_{AB}N > \chi_{BC}N$, the KP phase can become stable instead of $C_4^{(a)}$ and PL. On the other hand, a noticeable stable region of the KP phase, with respect to f_A and ε_B, has been obtained for $f_B = 0.22$, $\varepsilon_C = 1$ and symmetric interaction parameters $\chi_{AB}N = \chi_{BC}N = 60$. This suggests that the relative stability of the KP phase is strongly dependent on not only the relative strength of interaction parameters, but also the conformational parameters. Finally, we choose a specific set of parameters characterizing the SEBM samples and compute a complete stable phase region of the KP phase which is surrounded by the neighboring phases of LC, PL, L_3, CSC, PC, and $C_4^{(a)}$. This phase region with a considerable area is rather close to where the KP phase was observed in experiments. Furthermore, the phase diagram can serve as a guide for experiments to obtain stable KP morphology, e.g., by simply using smaller PEB block. Our comprehensive study could provide further understanding on the emergence and stability of the KP phase, one of the most intriguing unconventional phases.

AUTHOR INFORMATION

Corresponding Author

*E-mail: weihuali@fudan.edu.cn.

Notes

The authors declare no competing financial interest.

ACKNOWLEDGMENTS

This work was supported by the National Natural Science Foundation of China (Grants 20974026 and 21174031), the National High Technology Research and Development Program of China (863 Grant 2008AA032101), and the Natural Science and Engineering Research Council (NSERC) of Canada.

REFERENCES

(1) Park, S.; Wang, J. Y.; Kim, B.; Xu, J.; Russell, T. P. *ACS Nano* **2008**, *2*, 766.
(2) Hsu, J.-C.; Liu, C.-L.; Chen, W.-C.; Sugiyama, K.; Hirao, A. *Macromol. Rapid Commun.* **2011**, *32*, 528.
(3) Thurn-Albrecht, T.; Schotter, J.; Kastle, G. A.; Emley, N.; Shibauchi, T.; Krusin-Elbaum, L.; Guarini, K.; Black, C. T.; Tuominen, M. T.; Russell, T. P. *Science* **2000**, *290*, 2126.
(4) Lee, J. I.; Cho, S. H.; Park, S. M.; Kim, J. K.; Kim, J. K.; Yu, J. W.; Kim, Y. C.; Russell, T. P. *Nano Lett.* **2008**, *8*, 2315.
(5) Matsen, M. W.; Schick, M. *Phys. Rev. Lett.* **1994**, *72*, 2660.
(6) Tyler, C. A.; Morse, D. C. *Phys. Rev. Lett.* **2005**, *94*, 208302.
(7) Ungar, G.; Tschierske, C.; Abetz, V.; Holyst, R.; Bates, M. A.; Liu, F.; Prehm, M.; Kieffer, R.; Zeng, X.; Walker, M.; Glettner, B.; Zywocinski, A. *Adv. Funct. Mater.* **2011**, *21*, 1296.
(8) Qian, H. J.; Lu, Z. Y.; Chen, L. J.; Li, Z. S.; Sun, C. C. *Macromolecules* **2005**, *38*, 1395.
(9) Bailey, T. S. Morphological behavior spanning the symmetric AB andABC block copolymer states. Ph.D. Thesis, University of Minnesota, 2001.
(10) Stadler, R.; Auschra, C.; Beckmann, J.; Krappe, U.; Voigt-Martin, I.; Leibler, L. *Macromolecules* **1995**, *28*, 3080.
(11) Krappe, U.; Stadler, R.; Voigt-Martin, I. *Macromolecules* **1995**, *28*, 4558.
(12) Breiner, U.; Krappe, U.; Stadler, R. *Macromol. Rapid Commun.* **1996**, *17*, 567.
(13) Breiner, U.; Krappe, U.; Abetz, V.; Stadler, R. *Macromol. Chem. Phys.* **1997**, *198*, 1051.
(14) Breiner, U.; Krappe, U.; Jakob, T.; Abetz, V.; Stadler, R. *Polym. Bull.* **1998**, *40*, 219.
(15) Brinkmann, S.; Stadler, R.; Thomas, E. L. *Macromolecules* **1998**, *31*, 6566.
(16) Jinnai, H.; Kaneko, T.; Matsunaga, K.; Abetz, C.; Abetz, V. *Soft Matter* **2009**, *5*, 2042.
(17) Breiner, U.; Krappe, U.; Thomas, E. L.; Stadler, R. *Macromolecules* **1998**, *31*, 135.
(18) Auschra, C.; Stadler, R. *Macromolecules* **1993**, *26*, 2171.
(19) Ott, H.; Abetz, V.; Altstadt, V. *Macromolecules* **2001**, *34*, 2121.
(20) Elbs, H.; Abetz, V.; Hadziioannou, G.; Drummer, C.; Krausch, G. *Macromolecules* **2001**, *34*, 7917.
(21) Elbs, H.; Drummer, C.; Abetz, V.; Krausch, G. *Macromolecules* **2002**, *35*, 5570.
(22) Ludwigs, S.; Boker, A.; Abetz, V.; Muller, A. H. E.; Krausch, G. *Polymer* **2003**, *44*, 6815.
(23) Ludwigs, S.; Schmidt, K.; Stafford, C. M.; Amis, E. J.; Fasolka, M. J.; Karim, A.; Magerle, R.; Krausch, G. *Macromolecules* **2005**, *38*, 1850.
(24) Balsamo, V.; von Gyldenfeldt, F.; Stadler, R. *Macromolecules* **1999**, *32*, 1226.
(25) Nagpal, U.; Detcheverry, F. A.; Nealey, P. F.; de Pablo, J. J. *Macromolecules* **2011**, *44*, 5490.
(26) Zheng, W.; Wang, Z. G. *Macromolecules* **1995**, *28*, 7215.
(27) Tang, P.; Qiu, F.; Zhang, H. D.; Yang, Y. L. *Phys. Rev. E* **2004**, *69*, 031803.
(28) Guo, Z. J.; Zhang, G. J.; Qiu, F.; Zhang, H. D.; Yang, Y. L.; Shi, A. C. *Phys. Rev. Lett.* **2008**, *101*, 028301.
(29) Li, W. H.; Qiu, F.; Shi, A. C. *Macromolecules* **2012**, *45*, 503.
(30) Li, S. B.; Qiu, W. J.; Zhang, L. X.; Liang, H. J. *J. Chem. Phys.* **2012**, *136*, 124906.
(31) Tang, P.; Qiu, F.; Zhang, H. D.; Yang, Y. L. *J. Phys. Chem. B* **2004**, *108*, 8434.
(32) Bates, F. S.; Schulz, M. F.; Khandpur, A. K.; Forster, S.; Rosedale, J. H.; Almdal, K.; Mortensen, K. *Faraday Discuss.* **1994**, *98*, 7.
(33) Shi, A.-C. *Development in Block Copolymer Science and Technology*; Hamley, I. W., Ed.; Wiley: New York, 2004.
(34) Fredrickson, G. H. *The Equilibrium Theory of Inhomogeneous Polymers*; Oxford University Press: Oxford, UK, 2006.
(35) Goldacker, T.; Abetz, V. *Macromol. Rapid Commun.* **1999**, *20*, 415.
(36) Matsen, M. W.; Bates, F. S. *Macromolecules* **1996**, *29*, 7641.
(37) Matsen, M. W. *J. Chem. Phys.* **1998**, *108*, 785.
(38) Tyler, C. A.; Qin, J.; Bates, F. S.; Morse, D. C. *Macromolecules* **2007**, *40*, 4654.
(39) Matsen, M. W. *J. Phys.: Condens. Matter* **2002**, *14*, R21.
(40) Matsen, M. W.; Schick, M. *Macromolecules* **1994**, *27*, 4014.
(41) Vavasour, J. D.; Whitmore, M. D. *Macromolecules* **1993**, *26*, 7070.
(42) Vavasour, J. D.; Whitmore, M. D. *Macromolecules* **1996**, *29*, 5244.
(43) Matsen, M. W.; Bates, F. S. *J. Polym. Sci., Part B: Polym. Phys.* **1997**, *35*, 945.
(44) Stocker, W.; Beckmann, J.; Stadler, R.; Rabe, J. P. *Macromolecules* **1996**, *29*, 7502.
(45) Ballard, D. G. H.; Wignall, G. D.; Schelten, J. *Eur. Phys. J.* **1973**, *9*, 965.
(46) Kirste, R. G. *Makromol. Chem.* **1967**, *101*, 91.
(47) Bates, F. S.; Dierker, S. B.; Wignall, G. D. *Macromolecules* **1986**, *19*, 1938.